

# Influence of electron-electron interaction on the cyclotron resonance spectrum of magnetic quantum dots containing few electrons

Nga T. T. Nguyen<sup>1,\*</sup> and F. M. Peeters<sup>1,2,†</sup>

<sup>1</sup>*Departement Fysica, Universiteit Antwerpen, Groenenborgerlaan 171, B-2020 Antwerpen, Belgium*

<sup>2</sup>*Departamento de Física, Universidade Federal do Ceará, Caixa Postal 6030, Campus do Pici, 60455-760 Fortaleza, Ceará, Brazil*

(Received 26 February 2010; revised manuscript received 9 January 2011; published 22 February 2011)

The configuration interaction method is used to obtain the magneto-optical absorption spectrum of a few-electron ( $N_e = 1, 2, \dots, 5$ ) quantum dot containing a single magnetic ion. We find that the IR spectrum (the position, the number, and the oscillator strength of the cyclotron resonance peaks) depends on the strength of the Coulomb interaction, the number of electrons, and the position of the magnetic ion. We find that the Kohn theorem is no longer valid as a consequence of the electron-spin-magnetic-ion-spin-exchange interaction.

DOI: [10.1103/PhysRevB.83.075419](https://doi.org/10.1103/PhysRevB.83.075419)

PACS number(s): 78.67.Hc, 71.55.Eq, 75.75.-c, 75.50.Pp

## I. INTRODUCTION

The magnetic properties of group II-VI semiconductor quantum dots (QDs) doped with magnetic impurities<sup>1</sup> have recently attracted considerable attention. Studies on those systems have led to fundamental insights in magnetism and resulted in, for example, different effective spin states.<sup>2</sup> Such a QD can exhibit robust magnetic-polaron behavior,<sup>3,4</sup> ferromagnetic/antiferromagnetic states,<sup>5-7</sup> piezomagnetism,<sup>8</sup> and shell structure,<sup>9-11</sup> which can be probed experimentally<sup>2,4,12-15</sup> and studied theoretically<sup>16-21</sup> through optical spectroscopy and FIR spectroscopy.<sup>22,23</sup>

Experimentally, one typically produces an ensemble of QDs which are doped with a very low concentration of Mn ions ( $\text{Mn}^{2+}$ ). Statistically, some of the QDs contain only a single magnetic ion, as was recently confirmed in a CdTe “artificial atom” deposited on a ZnTe substrate<sup>2</sup> by using molecular beam epitaxy growth. It is expected that such a hybrid QD structure is promising for different applications, for example, electronic and magnetic memories,<sup>24</sup> nanomagnets,<sup>25</sup> and quantum computing.

The Mn ion in a Cd(Mn)Te self-assembled QD is iso-electronic with the QD electrons and only interacts with these electrons via a zero-range spin-spin-exchange interaction that is  $J_c \vec{M} \cdot \vec{s}_i \delta(\vec{r}_i - \vec{R})$ . We recall that experimental IR spectroscopy of a few-electron  $\text{In}_x\text{Ga}_{1-x}\text{As}/\text{GaAs}$  QD without a magnetic impurity were conducted in, for example, Ref. 26 and studied theoretically in detail<sup>27</sup> for up to  $N_e = 6$  electrons. It was found that in a quadratically confined QD without impurities, the cyclotron resonance spectrum was independent of the number of electrons. This is the so-called “Kohn theorem” extended to quadratically confined QDs. Here we show that Kohn’s theorem breaks down in parabolic confined QDs when a magnetic impurity is present and that the cyclotron resonance spectrum changes qualitatively when the number of electrons is varied.

To date, the FIR magneto-optical spectrum of Cd(Mn)Te QDs containing few electrons has not yet been measured experimentally or calculated. In this paper we calculate the IR absorption spectrum in the presence of a magnetic field for a QD with  $N_e = 3, 4, 5$  electrons (the FIR spectroscopy for the cases  $N_e < 3$  can be found in Ref. 23), where electron transitions are possible beyond the  $s$  orbital. We consider in

detail the special case that the impurity is located at the center and off center [i.e.,  $(0.5l_0, 0)$ ,  $l_0$  is the parabolic-confinement length of the dot]. We show that by increasing the number of electrons, the magneto-optical spectrum changes significantly due to the shell-filling effect and the interaction of the electrons with the Mn ion. Furthermore, for  $N_e > 2$  electrons exhibit  $p$ - $p$  and even  $p$ - $d$  exchange coupling with the Mn ion leading to a larger number of electron-Mn-ion exchange couplings.

The structure of the paper is as follows. Section II presents the methodological approach and the most important results obtained for three, four, and five electrons are given. Section III concludes with the discussion on the influence of the electron-electron interaction and the number of electrons on the IR absorption spectrum of the system.

## II. MAGNETO-OPTICAL ABSORPTION ENERGY

### A. Cyclotron resonance method for few-electron QD doped with a single $\text{Mn}^{2+}$

We consider few interacting electrons confined by a parabolic potential with confinement strength  $\hbar\omega_0$  (tens of  $\text{meV}$ )<sup>9</sup> embedded in a quasi-two-dimensional CdTe host QD doped with a single Mn ion. The strength<sup>28</sup> of the electron-Mn-ion spin-spin-exchange interaction is typically about  $J_c = 1.5 \text{ eV}\text{\AA}^2$ . Here, we focus on many-body effects on the cyclotron resonance (CR) energy. For details on the methodology and the set of parameters used, we refer to Refs. 9 and 7. In a nutshell, we have adopted the configuration interaction (CI) method to build up the Hamiltonian<sup>9</sup> matrix and employ exact diagonalization<sup>7</sup> (ED) to obtain numerically the many-body eigenstates. Note that due to the spin-exchange interaction of the electrons with the Mn ion, the eigenvalue of the total angular momentum  $L$  and the total electron spin  $S_z$  are no longer good quantum numbers and the Hamiltonian needs to be built up in the entire Hilbert space. This rapidly increases the size of the Hamiltonian matrix, where the increase (a factor of six) due to the relatively large spin size  $5/2$  of the Mn ion has also to be taken into account. Substantial effort has to be made to numerically implement the diagonalization to obtain the FIR spectrum for  $N_e > 3$  electrons.

The oscillator strength (OS) of the intraband electron transitions (from ground state  $i$  to excited state  $j$ ) are calculated using the transition amplitude

$$A_{ij} = \sum_{p=1}^{N_e} \langle \Psi_i(\vec{r}_1, \dots, \vec{r}_{N_e}) | r_p e^{\pm i\theta_p} | \Psi_j(\vec{r}_1, \dots, \vec{r}_{N_e}) \rangle, \quad (1)$$

with its corresponding transition energy  $E_{ij} = E_j - E_i$ .  $\Psi_{i(j)}$  is the many-body wave function<sup>7</sup> of state  $i$  ( $j$ ), which is a linear combination of all possible  $N_e$  quantum state wave functions  $\psi_{i(j)}$  where  $\psi_{i(j)}$  is a product of electron Slater determinants and spin component of the Mn ion for configuration  $i$  ( $j$ ). The chosen basis consists of Fock-Darwin orbitals in a magnetic field (cyclotron frequency  $\omega_c$ ). We included a sufficiently large number of single-particle quantum states (Fock-Darwin levels) to ensure numerical convergency. All allowed transitions with OS exceeding 1% are retained. Notice that due to spin exchange of the different types of particles, different types of transitions where the  $z$  projection of the total spin of electrons and the spin of Mn ion balance each other become possible, leading to several CR peaks in the absorption spectrum.

The number of nonzero transition elements increases in the presence of a Mn ion as a consequence of the electron-spin-Mn-exchange interaction, which removes some selection rules. Moreover, different electrons in different orbital states lead to different allowed transitions.

The single-electron energy diagram in the case without a Mn-ion is depicted in Fig. 1 as function of the applied magnetic field. We indicated the allowed transitions by dash-dotted arrows for the case of two magnetic field values. We add the electron Zeeman term to the theoretical Fock-Darwin levels to distinguish the  $\pm 1/2$  spin states. Without the Mn-ion,

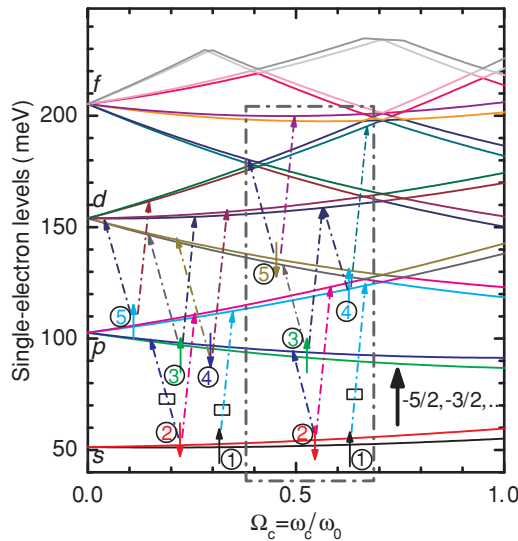


FIG. 1. (Color online) Single-particle energy levels (without Mn ion) and allowed electron transitions for two magnetic fields (separated by dash-dotted rectangular box) for  $N_e = 1-5$  electrons referred by numbers 1 to 5. The transitions are indicated by dash-dotted arrows colored, respectively, by the color of the final-state energy level. Big black arrow (bottom right) stands for a Mn ion with six possible  $M_z$  values. Transitions indicated by small enclosed rectangles become forbidden when  $N_e$  increases due to the Pauli exclusion principle.

the absorption spectra are independent of  $N_e$  for parabolic confinement due to Kohn theorem.<sup>29,30</sup>

We introduce right- and left- (circular-) polarized eigenmodes  $\sigma^-$  and  $\sigma^+$ , which, respectively, refer to right and left circular light.  $\sigma^-$  and  $\sigma^+$  connect the Fock-Darwin (initial and final) states with positive ( $\Delta l = 1$ ) and negative ( $\Delta l = -1$ ) difference of azimuthal quantum number, respectively. It is possible that  $\sigma^-$  ( $\sigma^+$ ) has different frequencies (absorption energy branches), say  $\sigma_{\alpha_1}^-$  ( $\sigma_{\alpha_1}^+$ ),  $\sigma_{\alpha_2}^-$  ( $\sigma_{\alpha_2}^+$ ),  $\dots$ , corresponding to the transition of different electrons. For simplicity in notation, we drop the subscripts  $\alpha_1, \alpha_2, \dots$  when classifying the right- (left-) polarized eigenmodes in the  $\sigma^-$  ( $\sigma^+$ ) group. Configuration information is included to clarify different electron transitions.

In our calculation of the absorption spectrum, we use a Lorentzian broadening  $\sigma_i(E) = \sum_j \{(\Gamma_{ij}/\pi) \cdot f_{ij}/[(E - E_{ij})^2 + \Gamma_{ij}^2]\}$ , allowing us to simultaneously observe the OS  $f_{ij} = 2\Delta E_{ij}/\hbar\omega_H \cdot |A_{ij}|^2/l_H^2$  and its transition energy  $E_j - E_i$ , where  $\Gamma_{ij}$  is taken to be  $10 \mu\text{eV}$ . We define  $\omega_H = \omega_0(1 + \Omega_c^2/4)^{1/2}$ , where  $\Omega_c = \omega_c/\omega_0$  is the hybrid frequency and  $l_H = [\hbar/(m_e^*\omega_H)]^{1/2}$  is the new length scale. The other parameters used in this paper are applicable to a  $\text{II}(\text{Mn})\text{VI Cd}(\text{Mn})\text{Te QD}$ , which has the Landé  $g$  factors  $g_e = -1.67$ ,  $g_{\text{Mn}} = 2.02$ , effective mass  $m_e^* = 0.106m_e$ , dielectric constant  $\epsilon = 10.6$ , and effective Bohr radius  $a_B^* = 52.9 \text{ \AA}$ . The ratio  $\lambda_C = l_0/a_B^*$  is defined as the Coulomb interaction strength.

## B. Numerical results

### 1. Three-electron QD

Given that the position of the Mn ion affects the electron-Mn-ion ferromagnetic-antiferromagnetic (FM-AFM) transition,<sup>7</sup> the CR spectrum of a three-electron QD for two typically different Mn-ion positions  $R_{\text{Mn}} = 0$  and  $R_{\text{Mn}} = 0.5l_0$  exhibits significant differences particularly in the presence of low-OS transitions as a consequence of the spin exchanges (see Figs. 2 and 3). The spin exchanges for the latter case ( $R_{\text{Mn}} = 0.5l_0$ ) are larger than that for the first case due to the absence of coupling between the  $s$  orbital with the  $p$  and  $d^\pm$  [ $(n_r, l) = (0, \pm 2)$ ] (as the lower states) orbitals when the Mn ion is located at the center of the dot. For the FM phase we have the spin state  $S_z = -1/2$  in the latter case which compares to  $1/2$  in the first case. As a consequence, its ground state has only the quantum state  $(n, L_z, S_z, M_z) = (0, 1, -1/2, -5/2)$  as its main contribution while  $(0, 1, 1/2, -5/2)$  and  $(0, 1, -1/2, -3/2)$  are the quantum states for the first case. Therefore, the number of allowed electron transitions from the ground state for the first case when the system is in the FM phase (six) is larger than that for the latter case (three or four), as can be seen from Figs. 2 and 3. The contribution  $(0, 1, -1/2, -3/2)$ , which becomes dominant in the excited-state wave function, is ascribed to the presence of the double right-polarized modes (of the spin-down  $s$  electron and spin-up  $p_{(n_r, l)=(0, 1)}^+$  electron) as peaks 1 and 2 and double left-polarized modes as the other two large-OS peaks (4 and 6) for  $\Omega_c = \omega_c/\omega_0 = 0.02$  ( $\approx 0.15 \text{ T}$ ). For  $\Omega_c = 0.1$ , this  $(0, 1, -1/2, -3/2)$  configuration is ascribed to the presence of the whole triple left-polarized modes as peaks II, III, and

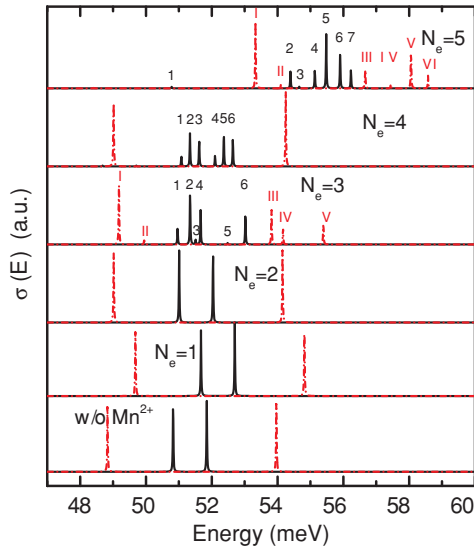


FIG. 2. (Color online) Magneto-optical absorption spectrum of a many-electron ( $N_e = 1-5$ ) QD for  $\Omega_c = 0.02$  (solid black curves) and  $0.1$  (dash-dotted red curves) in case the Mn ion is located at the center of the dot for  $\lambda_c = 0.5$ . Numbers are added on top of the CR peaks for distinguishability and for discussion. The absorption energy for the case without a Mn ion is plotted for reference (bottom figure).

IV (see Fig. 2). The very-low-OS (4% of the total OS) peak (number 3) is the left-polarized mode combining the  $\sigma^+(s)$  of the spin-down  $s$  electron and the  $p^+$  electron where the configuration  $(0, 1, -1/2, -3/2)$  strongly dominates the final state.

Increasing the field to  $\Omega_c = 0.1$  results in a change of the absorption spectrum as shown by the dash-dotted red curves in Fig. 2, where there is only one right-polarized mode (the largest-OS peak labeled by number I). The triple left-polarized modes are the CR lines that combine the  $\sigma^+(s)$  of, respectively, the two  $s$ -electron transitions and the spin-down  $s$ -electron

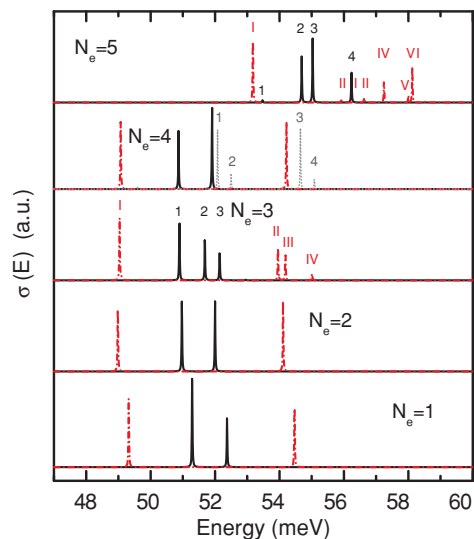


FIG. 3. (Color online) The same as Fig. 2 but for the case that the Mn ion is moved to  $(0.5l_0, 0)$ . For  $N_e = 4$  we added also the data for  $\Omega_c = 0.05$  by the gray dotted curve. The numbers on the top of each peak are given for distinguishability and for discussion.

and the  $p^+$ -electron transitions (double). In fact, the FM-AFM transition for  $R_{Mn} = 0$  and  $R_{Mn} = 0.5l_0$  occurs at, respectively,  $\Omega_c = 2.3$  and  $0.04$  (see Ref. 7). It means that one can observe the FM-AFM transition in the CR energy for the latter case in Fig. 3 as an increase in the number of CR peaks (from three to four). It is worth noting that with the presence of the Mn ion it now becomes possible to observe transitions of the different electrons, that is, different  $\sigma^+$  and  $\sigma^-$  (e.g., for  $\Omega_c = 0.1$ ), and the separation in energy will be much more pronounced for the highly polarized case. For  $R_{Mn} = 0.5l_0$  in the FM phase, the three peaks are the absorption energies from the right-polarized mode and the double left-polarized modes.

The number of CR peaks increases when the system transits to the AFM phase as can be seen from Figs. 2, 3, and 4. In the high-field region where only the spin-exchange interactions are active without changing  $M_z$  or  $S_z$ , the number of major CR peaks is four (Fig. 4), as compared to three for  $N_e = 2$ , which refers to the two modes ( $\sigma^-$ , second-largest-OS peak;  $\sigma^+$ , largest-OS peak) of the outermost electron and the other two ( $\sigma^+$ ) for the  $s$  electron (the third-largest-OS peak) and the  $p$  electron. Using the quantum-state wave function formalism, the ground state which has  $(n, L_z, S_z, M_z) = (0, 3, 3/2, -5/2)$  as its largest contribution will have four major electron transitions to  $(0, 3, 1/2, -5/2)$  ( $\sigma^-$ ),  $(1, 1, 1/2, -5/2)$  ( $\sigma^+$ ),  $(1, 0, 1/2, -5/2)$  ( $\sigma^+$ ), and  $(0, -1, 1/2, -5/2)$  ( $\sigma^+$ ). Note also that in the very-high-field limit, there is an influence of the exchange interaction on the CR spectrum, as seen in the separated peaks which merge in the absence of the Mn ion.

The polarized light couples only with the center-of-mass motion of the electrons. The above phenomenon where the different electron transitions of the three-electron QD are found to be different is a result of the coupling of the electron relative motions with their center-of-mass motion through the electron-Mn-ion spin-exchange interaction term. These spin-exchange elements depend on the quantum orbitals that the electrons occupy and on the position of the Mn ion inside the dot. This leads to a coupling that is different for different

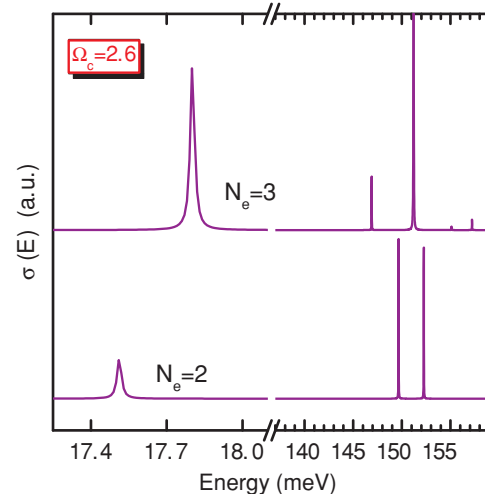


FIG. 4. (Color online) Magneto-optical absorption spectrum of a many-electron ( $N_e = 2$  and  $3$ ) QD at high magnetic field  $\Omega_c = 2.6$  ( $\approx 19.5$  T) in case the Mn ion is located at the center of the dot for  $\lambda_c = 0.5$ .

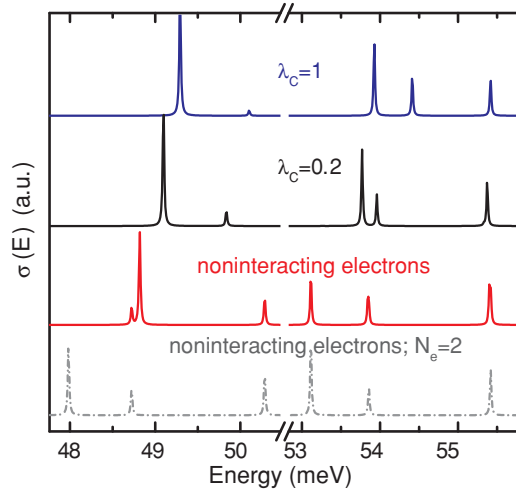


FIG. 5. (Color online) Coulomb interaction strength dependence of the magneto-optical absorption spectrum of a three-electron QD for  $\Omega_c = 0.1$  in case the Mn ion is located at the center of the dot. The absorption energy for the same QD in case without electron-electron interaction for  $N_e = 2$  electrons (dash-dotted line) is plotted for reference.

electrons. In addition, the electron-electron interaction now turns out to be important in characterizing the absorption spectrum because its form depends on the electron relative coordinate ( $\propto 1/|\vec{r}_{ij}^2|$ ). As proven for a two-electron QD,<sup>23</sup> the Coulomb repulsion “weakens” the spin-exchange interaction and reduces substantially the exchange energy contribution to the FIR spectrum as compared to that for the case of the noninteracting QD system. For  $2 < N_e < 6$  electrons, the ground state of the FM phase partially fills the  $p$  orbitals. The latter exhibits a maximum exchange energy for a Mn-ion position different from the center of the dot—the case for the  $s$  orbital ( $N_e \leq 2$  electrons). The  $\lambda_C$  dependence of the IR spectroscopy results in changes, as shown in Fig. 5 for  $\Omega_c = 0.1$ . The smaller  $\lambda_C$  the stronger the influence of the exchange energy on the electron transitions which results in almost equal large-OS peaks for the extreme case without electron-electron interaction. The smallest-OS peak discussed above for  $\lambda_C = 0.5$  becomes more pronounced for smaller  $\lambda_C$ . The influence of the Coulomb interaction on the IR spectroscopy will be further examined for  $N_e = 4$  and 5 electrons.

## 2. Four-electron QD

Next, we discuss in more detail the low-magnetic-field, say within the FM-state region, behavior of the four-electron QD system. Note that the FM-AFM transition magnetic field was found at  $\Omega_c = 3.87$  and 2.5 for  $R_{Mn} = 0$  and  $R_{Mn} = 0.5l_0$ , respectively. These transition magnetic fields are considered moderate as compared to the critical field at which the system becomes fully polarized. In the low-magnetic-field region, the CR peaks give us information on the spin exchange and are found as combinations of  $\sigma^+(s)$  or  $\sigma^-(s)$  for different electrons. These peaks only become more characteristic; that is, each of which corresponds to a different transition referred to a different electron orbital, with increasing field (as seen in the cases for  $N_e < 4$ ). For

$R_{Mn} = 0.5l_0$ , the system (in the FM phase) exhibits states  $S_z = -1$  ( $\Omega_c < 0.04$ ),  $S_z = 1$  ( $0.04 \leq \Omega_c < 0.1$ ), and 0 for the remaining FM region ( $0.1 \leq \Omega_c < 2.5$ ). The intermediate states are  $S_z = 1$  ( $\Omega_c < 0.1$ ) and 0 ( $0.1 \leq \Omega_c < 3.87$ ) for  $R_{Mn} = 0$ . Respectively, the number of CR peaks changes as shown in Figs. 2 and 3. This first intermediate FM state ( $S_z = 1$ ) in case  $R_{Mn} = 0$  exhibits six major transitions (three right- and left-polarized combined modes) where the larger the CR peaks, the more dominant is the contribution of the final-state configurations appropriate to the ground-state wave function consisting of  $(0,0,1, -5/2)$  (strongly dominant) and  $(0,0,0, -3/2)$  (slightly larger than 0). These transitions can be schematically described in the example inside the black dash-dotted rectangle in Fig. 1. The remaining intermediate state (for  $\Omega_c = 0.1$ ) has two large peaks that are the right- and left-polarized combined modes. Differences occur due to the position of the Mn ion, as illustrated in Fig. 3. The first intermediate FM state ( $S_z = -1$ ) exhibits two major transitions (for  $\Omega_c = 0.02$ ) while the second intermediate FM state ( $S_z = 1$ ) exhibits four major transitions (for  $\Omega_c = 0.05$ ). Differences induced by the Mn-ion position are found to be similar as in the  $N_e = 3$  case. The number of nonzero exchange elements increases reducing the energy difference in the resonant absorption energy. Consequently, for  $\Omega_c = 0.02$ , only single right-polarized and single left-polarized modes are recognizable, as shown in Fig. 3. For  $\Omega_c = 0.05$ , we have a very interesting situation. The system has both the properties of the previous case  $R_{Mn} = 0$  because of the same  $S_z = 1$  and the strong effective electron-Mn-ion interaction because of  $R_{Mn} = 0.5l_0$ . The ground-state mixes several quantum states of  $M_z = -1/2, -3/2$ , and  $-5/2$  ( $S_z + M_z = -3/2$ ). The number of major CR lines increases (four), as shown by the dotted gray curve in Fig. 3 with two right-polarized and two left-polarized combined modes.

We note that for an even number of electrons ( $N_e = 2, 4, \dots$ ) the FM phase generally is not as pronounced as that for the case of an odd number of electrons ( $N_e = 1, 3, 5, \dots$ ) and this fact leads to the appearance of only two major peaks (Figs. 2 and 3) for  $\Omega_c \geq 0.1$ . Apparently, Fermi-Dirac statistics plays an essential role because the filling effect, as seen clearly in case  $N_e = 4$  for the intermediate states  $S_z = \pm 1$  and 0, influences directly the spin-exchange interaction. To witness a stronger influence of the electron-Mn-ion interaction on the IR absorption spectrum for  $\Omega_c \geq 0.1$ , we refer to the AFM phase.

## 3. Five-electron QD

The IR absorption energies for  $N_e = 5$  are different for  $R_{Mn} = 0$  and  $R_{Mn} = 0.5l_0$  when the system is in the FM phase. This is similar to the case  $N_e = 3$  (see Refs. 9 and 7) where the system for small field ( $\Omega_c = 0.02$ ) for  $R_{Mn} = 0$  ( $S_z = 1/2$ ) reveals more peaks than for  $R_{Mn} = 0.5l_0$  ( $S_z = -1/2$ ) because of the spin-spin interaction. However, different from the case  $N_e = 3$  due to  $p$ - $p$  (orbital) electron-electron interaction effect, the absorption energies for  $N_e = 5$  are considerably different, for example, for  $\Omega_c = 0.02$ . A left-polarized mode can be at a smaller energy as compared to a right-polarized mode. This is illustrated in Fig. 2 where the left-polarized combined modes of the spin-down  $s$ -, spin-up  $p^+$ -, and

spin-up  $p^-$  electron and of the two spin-up  $p$  electrons are, respectively, peak 2 and peak 6. The remaining peaks 4, 5, and 7 are, respectively, the right-polarized CR lines of the three  $p$  electrons and the left-polarized CR line of the spin-down  $s$  electron and spin-up  $p^+$  electron. The same remark holds for  $R_{Mn} = 0.5l_0$  (Fig. 3) where the two largest-OS peaks (2 and 3 in Fig. 2) are the left-polarized absorption energies. At a larger field ( $\Omega_c = 0.1$ ), there is only one right-polarized CR line, which is peak I with the lowest transition energy. Three remaining large-OS peaks (IV, V, and VI) are the left-polarized modes combining the  $\sigma^+(s)$  of, respectively, the spin-down  $s$  electron and spin-up  $p^-$  electron, the two  $p^+$  electron and  $p^-$  electron, and the two  $s$  electrons and spin-up  $p^+$  electrons.

Besides the major CR peaks discussed above, we note the existence of the very-low-OS peaks ( $\approx 2\%$ – $5\%$  of the total OS) in all three cases of  $N_e$  that are an evidence of the influence of the electron-Mn-ion interaction when the small component to the ground state becomes the dominant one in the excited states. These peaks are peak 5 (for  $N_e = 3$ ) and peaks 1 and 3 (for  $N_e = 5$ ) in Fig. 2 and peak IV (for  $N_e = 3$ ) and peaks I, II, and III (for  $N_e = 5$ ) in Fig. 3.

### III. REMARKS AND CONCLUSIONS

Magneto-optical absorption energy of a parabolic many-electron QD in the presence of a magnetic impurity exhibits a lot of anticrossings/crossings in the energy spectrum due to the interplay of the different spin-exchange contributions. Consequently: (1) different electron transitions are found, for example, when the magnetic impurity is located at the center of the dot for  $N_e > 2$ , and (2) there are low-OS CR peaks along with the conventional ones. Positioning the Mn ion

off-center of the dot (i) increases the number of nonzero exchange interaction elements and (ii) can lead to a reduction in the energy difference between the CR lines. This results in a decrease in the number of CR peaks and one CR peak becomes a sum of the same type (right-/left-polarized) of absorption mode for different electrons. Electron-electron interaction in a few-electron QD doped with a single magnetic impurity considerably affects the system IR absorption spectrum by changing the number and strength of electron transitions. The reason is that the center-of-mass motion now couples differently with the relative motions and also with the Mn-ion coordinate in the electron-Mn-ion spin-exchange expression. Because the relative motions contain information about the electron-electron interaction, this fact leads to the existence of various IR absorption spectra for different numbers of electrons. Plus, many transitions of different electrons now have different energy. In the high-magnetic-field limit (strongly polarized electron system) different (lowest-Landau-level) electrons have separate transition energies and each time the number of electrons increases by one the number of major CR peaks increases by one, for example, from three (for  $N_e = 2$ ) to four (for  $N_e = 3$ ). Combined (right- or left-polarized) electron CR-lines reduce their contributions to zero. Only CR lines that correspond to essential right- or left-polarized modes, that is, each of which refers to a specific transition energy with a unique final state, are possible.

### ACKNOWLEDGMENTS

This work was supported by FWO-VI (Flemish Science Foundation), the Brazilian science foundation CNPq, and the Belgian Science Policy (IAP).

\*nga.nguyen@ua.ac.be; Present address: Condensed Matter Theory Center, Department of Physics, University of Maryland, College Park, Maryland 20742-4111, USA.

†francois.peeters@ua.ac.be

<sup>1</sup>J. K. Furdyna, *J. Appl. Phys.* **65**, 29 (1988).

<sup>2</sup>L. Besombes, Y. Léger, L. Maingault, D. Ferrand, H. Mariette, and J. Cibert, *Phys. Rev. Lett.* **93**, 207403 (2004).

<sup>3</sup>A. K. Bhattacharjee, *Phys. Rev. B* **35**, 9108 (1987).

<sup>4</sup>I. R. Sellers, R. Oszwałdowski, V. R. Whiteside, M. Eginligil, A. Petrou, I. Zutic, W.-C. Chou, W. C. Fan, A. G. Petukhov, S. J. Kim, A. N. Cartwright, and B. D. McCombe, *Phys. Rev. B* **82**, 195320 (2010).

<sup>5</sup>R. M. Abolfath, P. Hawrylak, and Igor Žutić, *Phys. Rev. Lett.* **98**, 207203 (2007).

<sup>6</sup>F. Qu and T. Vasilopoulos, *Appl. Phys. Lett.* **89**, 122512 (2006).

<sup>7</sup>N. T. T. Nguyen and F. M. Peeters, *Phys. Rev. B* **78**, 045321 (2008).

<sup>8</sup>R. M. Abolfath, A. G. Petukhov, and Igor Žutić, *Phys. Rev. Lett.* **101**, 207202 (2008).

<sup>9</sup>F. Qu and P. Hawrylak, *Phys. Rev. Lett.* **95**, 217206 (2005); **96**, 157201 (2006).

<sup>10</sup>Y. Léger, L. Besombes, J. Fernández-Rossier, L. Maingault, and H. Mariette, *Phys. Rev. Lett.* **97**, 107401 (2006).

<sup>11</sup>N. T. T. Nguyen and F. M. Peeters, *Phys. Rev. B* **76**, 045315 (2007).

<sup>12</sup>L. Besombes, Y. Léger, L. Maingault, D. Ferrand, H. Mariette, and J. Cibert, *Phys. Rev. B* **71**, 161307(R) (2005).

<sup>13</sup>C. Le Gall, L. Besombes, H. Boukari, R. Kolodka, J. Cibert, and H. Mariette, *Phys. Rev. Lett.* **102**, 127402 (2009).

<sup>14</sup>D. E. Reiter, T. Kuhn, and V. M. Axt, *Phys. Rev. Lett.* **102**, 177403 (2009); M. Goryca, T. Kazimierzczuk, M. Nawrocki, A. Golnik, J. A. Gaj, P. Kossacki, P. Wojnar, and G. Karczewski, *ibid.* **103**, 087401 (2009).

<sup>15</sup>G. Bacher, M. K. Welsch, A. Forchel, Y. Lyanda Geller, T. L. Reinecke, C. R. Becker, and L. W. Molenkamp, *J. Appl. Phys.* **103**, 113520 (2008).

<sup>16</sup>A. O. Govorov, *Phys. Rev. B* **70**, 035321 (2004).

<sup>17</sup>J. Fernández-Rossier, *Phys. Rev. B* **73**, 045301 (2006).

<sup>18</sup>K. Chang, J. B. Xia, and F. M. Peeters, *Appl. Phys. Lett.* **82**, 3570 (2003).

<sup>19</sup>S. J. Cheng, *Phys. Rev. B* **72**, 235332 (2005); **77**, 115310 (2008).

<sup>20</sup>J. van Bree, P. M. Koenraad, and J. Fernández-Rossier, *Phys. Rev. B* **78**, 165414 (2008).

<sup>21</sup>A. O. Govorov, *C. R. Phys.* **9**, 857 (2008).

<sup>22</sup>I. Savić and N. Vukmirović, *Phys. Rev. B* **76**, 245307 (2007).

<sup>23</sup>N. T. T. Nguyen and F. M. Peeters, *Phys. Rev. B* **78**, 245311 (2008); **80**, 115335 (2009).

- <sup>24</sup>A. O. Govorov and A. V. Kalameitsev, *Phys. Rev. B* **71**, 035338 (2005).
- <sup>25</sup>J. Fernández-Rossier and Ramón Aguado, *Phys. Rev. Lett.* **98**, 106805 (2007).
- <sup>26</sup>H. Drexler, D. Leonard, W. Hansen, J. P. Kotthaus, and P. M. Petroff, *Phys. Rev. Lett.* **73**, 2252 (1994).
- <sup>27</sup>A. Wojs and P. Hawrylak, *Phys. Rev. B* **53**, 10841 (1996).
- <sup>28</sup>J. Fernández-Rossier and L. Brey, *Phys. Rev. Lett.* **93**, 117201 (2004).
- <sup>29</sup>W. Kohn, *Phys. Rev.* **123**, 1242 (1961).
- <sup>30</sup>F. M. Peeters, *Phys. Rev. B* **42**, 1486 (1990).